Nonlinear Dyn
DOI 10.1007/s11071-016-2790-5

ORIGINAL PAPER

A semi-physical model for pneumatic control valves

Lei Fang · Li Tang · Jiandong Wang · Qunli Shang

Received: 10 May 2015 / Accepted: 10 April 2016

Abstract Pneumatic control valves in practice are usually composed of three signal conversion processes that are associated with significant nonlinearities and dynamics. However, several physical, semi-physical, and data-driven models in the literature describe only one signal conversion process from the actuator force to the valve stem position. In this paper, a semi-physical model is proposed based on the physical principles of the three signal conversion processes. The proposed model contains two new components, namely, a backlash nonlinearity in the electric-pneumatic conversion process and an input-direction-dependent dynamics in the pneumatic-force conversion process. In addition, an updated model for the force-position conversion process is shown to be overdamped, instead of being the underdamped one in the literature. Experimental studies are provided to support the proposed semi-physical model and demonstrate the discrepancies of representatives of existing physical, semi-physical and data-driven models with experimental observations.

Keywords Pneumatic control valve · Semi-physical model · Control loop performance

1 Introduction

Industrial process plants consist of numerous control loops to keep the important process variables such as pressure, flow, level and temperature within the required operating ranges to ensure the product quality [19]. The most common final control element in these process control loops is the control valve, which manipulates fluids to compensate the negative effects of disturbances and keep the controlled process variables close to desired setpoint values. Industrial surveys reported that about 20–30 % of control loops in process industries perform poorly due to control valve nonlinearities [2,6]. Among the control valves, the pneumatic control valves are most frequently used in practice [14]. Thus, it is practically important to establish an accurate model for pneumatic control valves in order to measure and compensate their negative effects on control loops.

The control valve models in the literature can be classified into the physical, data-driven and semi-physical models. The physical models are based on physics of friction forces and Newton's second law of motion. There are mainly four physical models,

This work was supported in part by the National Natural Science Foundation of China (Nos. 61061130559 and 61174108).

L. Fang and L. Tang have contributed equally to this paper.

L. Fang · L. Tang · J. Wang (✉)
College of Engineering, Peking University,
Beijing 100871, China
e-mail: jiandong@pku.edu.cn

Q. Shang
College of Information Engineering, Zhejiang University of Technology, Hangzhou 310014, China

Published online: 22 April 2016

namely, classical model [20,21], Karnopp model [17], seven parameter model [1] and Lugre model [5]. Among them, Karnopp model perhaps is the most widely accepted one for modeling control valves [4, 11,18]. The data-driven models are developed from output and input data samples of control valves, and are mainly motivated by detection and quantification of control valve stiction [15]. The data-driven models mainly include Stenman model [22], Choudhury model [4], Kano model [16], He model [10], Chen model [3] and XCH model [25]. Kano model and XCH model are two improved versions of Choudhury model having two parameters S and J, in order to deal with stochastic signals. He model also has two parameters f_s and f_d, but is different from Choudhury model in terms of a phenomenon that the control valve stops (instead of continuously varying) after each valve movement. Chen model is an extension of He model to address more state transitions. He model is reduced to Stenman model for the special case of $f_s = d$ and $f_d = 0$. Developed on the basis of both physical and data-driven models, He's semi-physical model [9,11] has three parameters K_1, f_{s1} and f_{d1}. He's semi-physical model has the same valve signature with He model, when the parameters satisfy the relations $f_d = f_{d1} - (K_1 - 1)(f_{s1} - f_{d1})$ and $f_s = f_{s1}$. In this sense, He model is a special case of He's semi-physical model. Therefore, Karnopp model, Kano model and He's semi-physical model are regarded as the representatives of the existing physical, data-driven, and semi-physical models, respectively.

A common limitation of the above models is that the actuator force, resulting from the air pressure on the diaphragm inside the valve actuator chamber, is taken as the model input. However, the air pressure in the valve actuator chamber cannot be directly manipulated in practice; instead, it is adjusted by a valve positioner. The valve positioner receives an electric signal from the controller in industrial distributed control systems, and changes the inlet air pressure accordingly into the valve actuator chamber. The air pressure inside the valve actuator chamber changes gradually with the inlet air pressure, and works on the diaphragm to form the actuator force. The actuator force overcomes various friction forces and determines the valve stem position. Therefore, three signal conversion processes are involved, namely, the electric-pneumatic, pneumatic-force and force-position conversion processes. The existing models ignore the dynamics and nonlinearities of the first two signal conversion processes and treat the electric signal the same as the actuator force. As a result, the existing models have large discrepancies with the actual behavior of a pneumatic control valve, shown later by experimental studies.

In this paper, a novel semi-physical model is proposed for pneumatic control valves to describe the relation between the electric control signal as model input and the valve stem position as model output, based on the physical principles of three signal conversion processes. Compared with the above-mentioned models in the literature, the proposed model has two new components, namely, a backlash nonlinearity for the electric-pneumatic conversion process and an input-direction-dependent dynamics for the pneumatic-force conversion process, as well as one updated model for the force-position conversion process showing overdamped dynamics. The behavior of the proposed model is consistent with experimental observations on a pneumatic control valve. By contrast, the representative existing models have large discrepancies with experimental observations.

The rest of the paper is organized as follows. Section 2 proposes the novel semi-physical model. Section 3 validates the proposed model via experimental studies, and compares it with Karnopp model, Kano model and He's semi-physical model. Section 4 gives some concluding remarks.

2 Modeling the pneumatic control valves

This section introduces the configuration of pneumatic control valves, and proposes a novel semi-physical model based on the physical principles of three signal conversion processes.

2.1 Configuration of a pneumatic control valve

The configuration of a pneumatic spring-diaphragm sliding-stem control valve is shown in Fig. 1. It mainly consists of three components, namely, the valve positioner, valve actuator and valve body. In this context, let us consider a microprocessor-based smart valve positioner whose usage in process industries has greatly increased in the last decade [8,19]. Thus, there is a feedback control loop as depicted in Fig. 2. Due to technical confidentiality, however, the control algorithms embedded in the smart valve positioner are usually unacces-

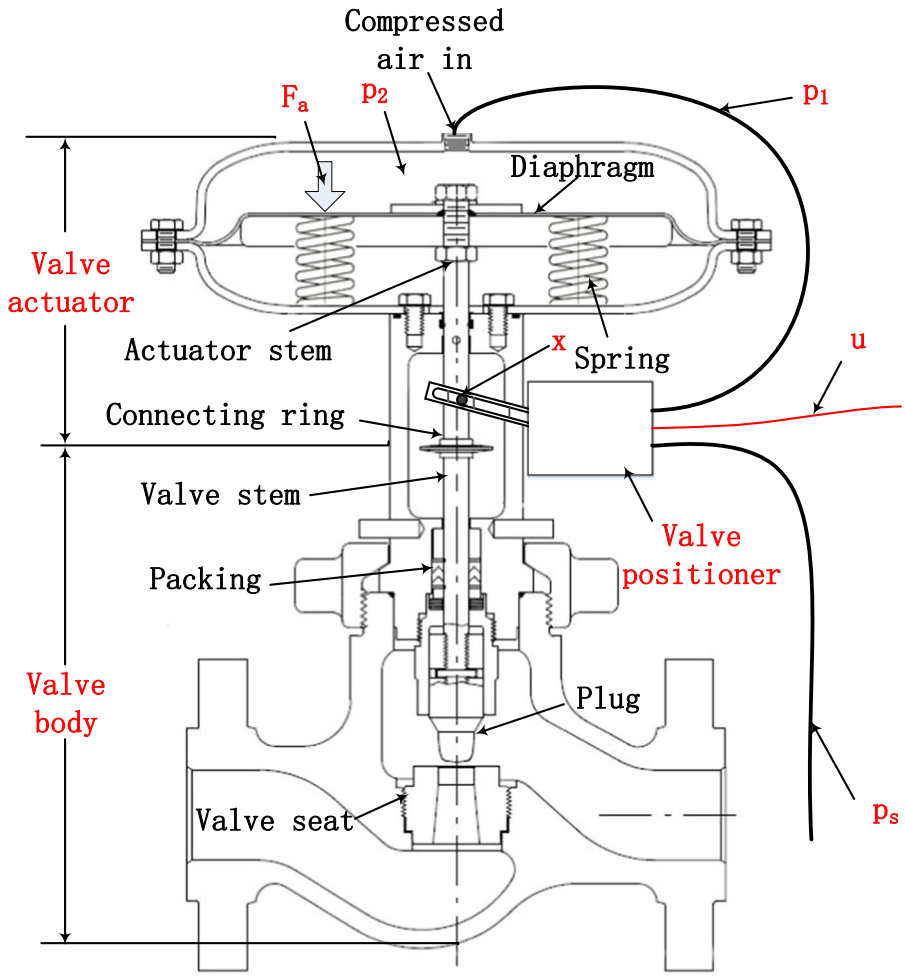

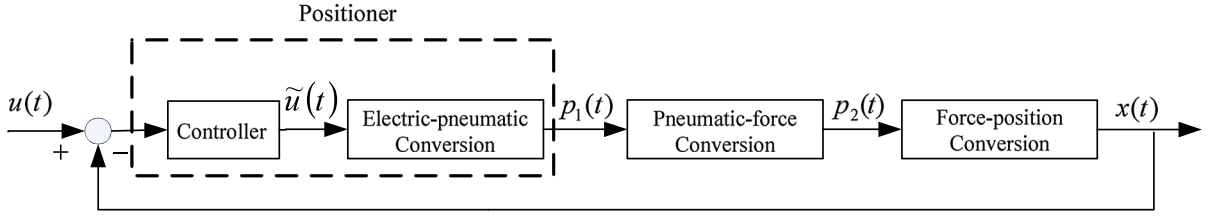

Fig. 1 Configuration of a pneumatic spring-diaphragm sliding-stem control valve

Fig. 2 Control loop diagram of the pneumatic control valve with a smart positioner

sible to the users. As a result, we disconnected the controller from the physical electric-pneumatic conversion device, and connected the electric control signal u directly to the electric-pneumatic conversion device, i.e., $\tilde{u}(t) = u(t)$. That is, u is applied to the pins of the nozzle–flapper-structured I/P converter in the valve positioner (illustrated later in Sect. 2.2.1) to change the inlet air pressure p_1 into the valve actuator chamber accordingly. The air pressure p_2 inside the valve actuator chamber, defined by p_1, is imposed on the diaphragm to form the actuator force F_a, which overcomes the spring and friction forces, moves the valve stem, and determines the final valve position x. Our objective is to build a mathematical model of the pneumatic control valves in such an open operation, in order to design advanced controllers to overcome the valve nonlinearities and improve the valve dynamic performance in future studies.

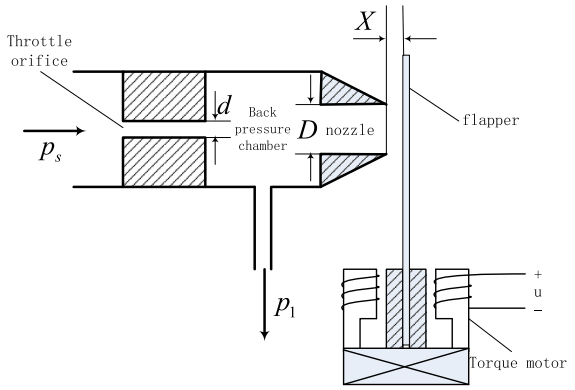

Fig. 3 A nozzle–flapper-structured I/P converter in the valve positioner

2.2 Signal conversion processes

Pneumatic control valves involve three signal conversion processes, namely, an electric-pneumatic conversion process from u to p_1, a pneumatic-force conversion process from p_1 to F_a, and a force-position conversion process from F_a to x. This subsection establishes the mathematical models for the three signal conversion processes based on the involved physical principles.

2.2.1 Electric-pneumatic conversion process

The electric-pneumatic conversion process is usually achieved by an I/P converter inside the valve positioner. A nozzle–flapper-structured I/P converter, as shown in Fig. 3, is one commonly used electric-pneumatic converter owing to the structural simplicity and low cost [19]. The compressed air with a constant pressure p_s from an air storage vessel goes through the throttle orifice and reaches the back pressure chamber. The compressed air continuously runs through the nozzle and injects into the flapper. The diameters of the throttle orifice and nozzle are about 0.2–0.5 mm and 0.8–2 mm, respectively. The torque motor directly receives the electric control signal u, and moves the flapper accordingly to vary the distance X between the nozzle and flapper. A force balance in the back pressure chamber is achieved to form the pressure p_1 of the back pressure chamber. The distance X is small so that it varies in an approximately linear relationship with respect to u. Clearly, if X is increased (decreased) by the torque motor, more (less) compressed air goes into the atmosphere through the gap between the nozzle and flapper so that p_1 is decreased (increased), too. The transient dynamics between X and p_1 can be ignored, since the back pressure chamber has a small volume. However, a backlash nonlinearity exists in the torque motor owing to its mechanical structure, and cannot be ignored as shown later in the experimental results in Sect. 3. Hence, after normalizing u and p_1 into the interval [0, 100 %], the relationship between u and p_1 is represented by a discrete time backlash model,

$$p_1(t) = \begin{cases} u(t) - f_{d1}, \text{ if } u(t) - p_1(t-1) > f_{d1}, \\ u(t) + f_{d1}, \text{ if } u(t) - p_1(t-1) < -f_{d1}, \\ p_1(t-1), \text{ if } |u(t) - p_1(t-1)| \le f_{d1}, \end{cases} \tag{1}$$

where f_{d1} is the backlash width parameter.

2.2.2 Pneumatic-force conversion process

The pneumatic-force conversion process describes the dynamics from the pressure p_1 to the actuator force F_a on the diaphragm inside the valve actuator chamber as shown in Fig. 4. The actuator force F_a is proportional to the air pressure p_2 inside the valve actuator chamber, i.e.,

$$F_a = Sp_2, \tag{2}$$

where the constant S is the area of the diaphragm. Thus, besides F_a, p_2 can also be taken as the model output for the pneumatic-force conversion process. When the air flow rate Q is not high, there is an approximately linear relationship between Q and the pressure difference $p_1 - p_2$ [13,23], i.e.,

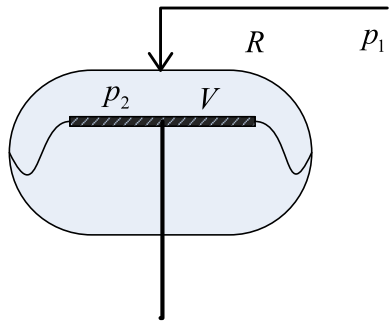

Fig. 4 Diaphragm-type pneumatic valve actuator

$$Q = \frac{p_1 - p_2}{R}, \tag{3}$$

where the constant R represents the air resistance. According to the ideal gas law, we have

$$p_2 V = k_T N. \tag{4}$$

Here V is the chamber volume, N is the amount of gas in the valve chamber, and k_T is a constant. When the valve position x moves around a steady-state value, the chamber volume V can be regarded as a constant. By using (3) and (4), the relation $Q = \frac{dN}{dt}$ leads to

$$\frac{V}{k_T}\frac{dp_2}{dt} = \frac{p_1 - p_2}{R}.$$

Hence, the relationship between p_1 and p_2 can be approximated by a first-order linear time-invariant model,

$$\frac{P_2(s)}{P_1(s)} = \frac{1}{\frac{RV}{k_T}s + 1}.$$

where $P_1(s)$ and $P_2(s)$ are the Laplace transforms of $p_1(t)$ and $p_2(t)$, respectively. However, the mechanisms of increasing and decreasing p_2 are different. When p_2 is increased, the compressed air is injected from the compressed air source via the nozzle–flapper-structured I/P converter to the valve actuator chamber under a higher back pressure p_1 generated by a closer distance X. When p_2 is decreased, the compressed air in the valve actuator chamber is discharged to the atmosphere via the gap between the nozzle and flapper. Hence, the air resistance R for injecting air is larger than the counterpart for discharging air in the valve actuator chamber. This fact leads us to define two different time constants $T_{g1} := \frac{R_1 V}{k_T}$ and $T_{g2} := \frac{R_2 V}{k_T}$ for the injecting and discharging processes, respectively. Then, the dynamics of the pneumatic-force conversion process depends on the direction of p_1 and can be presented in discrete time as

$$p_2(t) = \begin{cases} p_1(t-1) + [p_2(t-1) - p_1(t-1)]\exp\left(-T_s/T_{g1}\right), & \text{if } p_1(t) > p_2(t-1), \\ p_1(t-1) + [p_2(t-1) - p_1(t-1)]\exp\left(-T_s/T_{g2}\right), & \text{if } p_1(t) \le p_2(t-1). \end{cases} \tag{5}$$

Here T_s is the sampling period, and a zero-order holder is assumed to be used between two adjacent samples of $p_1(t)$.

2.2.3 Force-position conversion process

The force-position conversion process converts the pneumatic actuator force F_a, or equivalently the air pressure p_2 owing to (2), to the valve position x. A mass-spring system based on Karnopp model [4,9,11,17,18] is adapted here to model the force-position conversion process.

Based on Newton's second law of motion and balance of forces, the motion equations of the valve stem are

$$\dot{x} = v, \tag{6a}$$

$$m\dot{v} = F_a + F_r + F_f + F_p + F_i. \tag{6b}$$

Here the two state variables x and v are the position and velocity of the valve stem, respectively; m is the mass of the moving components in a pneumatic control valve. The spring force is

$$F_r = -kx, \tag{7}$$

where k stands for the spring constant. Both the force F_p due to the fluid pressure drop and the extra force F_i required to compel the valve stem plug into the seat are assumed to be zero due to their negligible contributions [18]. The friction force F_f is mainly from the tight seal between the valve stem and the valve body to avoid fluid leakage. Thus, F_f is composed of the Coulomb, viscous and Stribeck friction forces, i.e.,

$$F_f = \begin{cases} -F_c \text{sign}(v) - vF_v - (F_s - F_c)\exp\left[-(v/v_s)^2\right]\text{sign}(v), & \text{if } v \neq 0, \\ -(F_a + F_r), & \text{if } v = 0 \text{ and } |F_a + F_r| \le F_s, \\ -F_s \text{sign}(F_a + F_r), & \text{if } v = 0 \text{ and } |F_a + F_r| > F_s, \end{cases} \tag{8}$$

where v_s is the Stribeck velocity. The two terms $F_c \text{sign}(v)$ and vF_v are the Coulomb friction (also referred to as the dynamic friction) and viscous friction, respectively. The Stribeck friction $(F_s - F_c)\exp\left[-(v/v_s)^2\right]\text{sign}(v)$ describes that the friction force F_f decreases continuously from the static friction F_s to the dynamic friction F_c when the valve stem starts to move. When the valve stem moves, its velocity v is usually much larger than v_s. Consequently, the Stribeck friction has a negligible contribution. Note that the numerical simulation of (8) may encounter difficulties, because it is discontinuous at the zero velocity. To deal with this issue, a small dead zone $|v| < \delta_0 = 10^{-4}$ m/s is used as a numerical approximation of $v = 0$ [17]. Moreover, the parameters are usually normalized into dimensionless quantities in the range [0, 100 %]. Define the maximum position of the valve stem as x_m. Then, the parameters can be normalized as

$$\bar{x} = \frac{x}{x_m}, \quad \bar{p}_2 = \frac{Sp_2}{kx_m}, \quad f_s = \frac{F_s}{kx_m}, \quad f_d = \frac{F_c}{kx_m},$$
$$a_1 = \frac{k}{m}, \quad a_2 = \frac{F_v}{m}, \quad \delta = x_m\delta_0. \tag{9}$$

With a little abuse of notation, the symbols x and p_2 are still used hereafter to respectively represent $\bar{x}$ and $\bar{p}_2$. Based on (2), (6), (7), (8) and (9), we are ready to obtain a continuous-time model for the force-position conversion process,

$$\ddot{x} = \begin{cases} a_1(p_2 - x - f_d) - a_2\dot{x}, & \text{if } \dot{x} \geq \delta, \\ a_1(p_2 - x - f_s), & \text{if } -\delta < \dot{x} < \delta \text{ and } (p_2 - x) > f_s, \\ 0, & \text{if } -\delta < v < \delta \text{ and } -f_s \leq (p_2 - x) \leq f_s, \\ a_1(p_2 - x + f_s), & \text{if } -\delta < \dot{x} < \delta \text{ and } (p_2 - x) < -f_s, \\ a_1(p_2 - x + f_d) - a_2\dot{x}, & \text{if } \dot{x} \leq -\delta. \end{cases} \tag{10}$$

The discrete time implementation of (10) is given as Part 3 of the flowchart in Fig. 5.

2.3 Establishment of a semi-physical model

Based on the analysis of the three conversion processes in Sect. 2.2, a novel semi-physical model can be established for pneumatic control valves. The flow chart of the proposed model is shown in Fig. 5, composed of three parts. Part 1 represents the backlash nonlinearity (1) in the electric-pneumatic conversion process, where the model parameter is the backlash width f_{d1}. Part 2 is the input-direction-dependent dynamics of the pneumatic-force conversion process in (5) with the parameters T_{g1} and T_{g2}. Part 3 is the force-position conversion process in (10) with the parameters f_s, f_d, a_1 and a_2.

3 Experimental studies

This section presents experimental studies to validate the proposed semi-physical model, with a comparison with the representatives of the physical, data-driven, and semi-physical stiction models, namely, Karnopp model [17], Kano model [16] and He's semi-physical model [9].

3.1 Experimental setup

The experimental devices are shown in Fig. 6. The leftmost valve is the one used in the experiment. The valve positioner with the nozzle–flapper-structured I/P converter is connected with the compressed air source via an air source conduit. The positioner receives the electric control signal u from a signal generator in a computer via Matlab® Instrument Control Toolbox, and sends the compressed air via the inlet conduit to the valve chamber. A pressure sensor measures the air pressure p_2 inside the valve chamber. A position sensor measures the valve position x. Thus, the measurements of u, p_2 and x are available in the experiment, with the sampling period $T_s = 0.2$ sec. The signals u, p_2 and x are normalized to the range [0, 100 %] via a baseline test [7,12]; the percentage symbol % will be omitted hereafter for the notation convenience.

3.2 Parameter identification

The semi-physical model has seven parameters to be estimated, namely, $f_{d1}, T_{g1}, T_{g2}, f_s, f_d, a_1$ and a_2. The

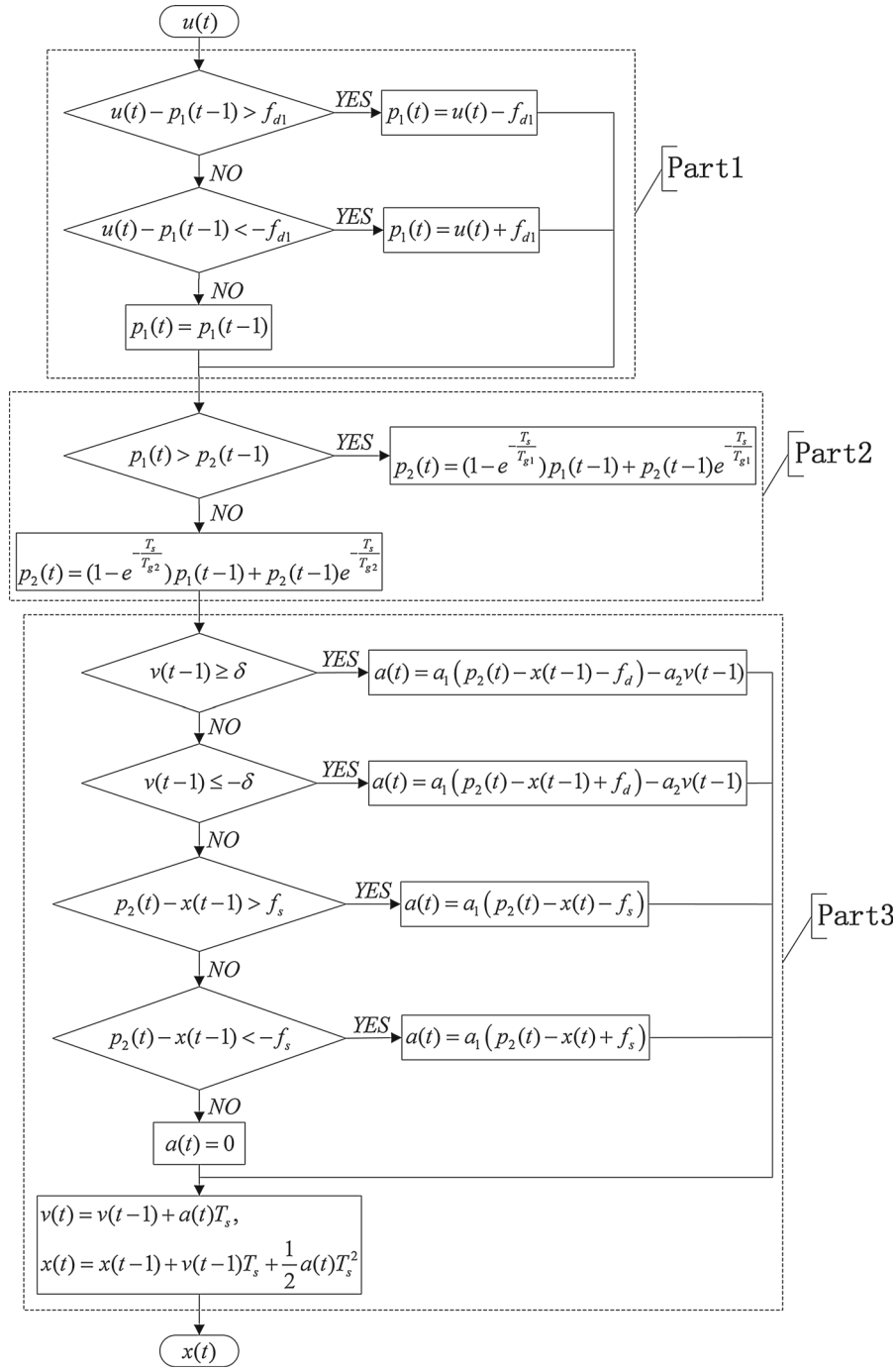

Fig. 5 Flow chart of the proposed semi-physical model for pneumatic control valves

estimation is based on maximizing the fitness between the actual valve output x and its estimated value $\hat{x}$ from the semi-physical model defined as

$$\eta = \left(1 - \frac{||x - \hat{x}||^2}{||x - \bar{x}||^2}\right) \times 100\,\%, \tag{11}$$

where $\bar{x}$ stands for the sample mean of x. For the pneumatic control valve in the experimental studies, the estimated parameters from some observed experimental data samples are

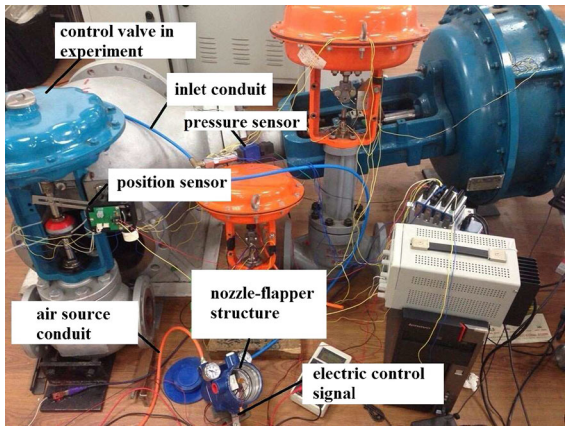

Fig. 6 The experimental devices

$$\hat{f}_{\mathrm{d1}} = 1.7647,\ \hat{T}_{\mathrm{g1}} = 8.84\ \mathrm{s},\ \hat{T}_{\mathrm{g2}} = 150.74\ \mathrm{s},$$
$$\hat{f}_{\mathrm{s}} = 8.7978,\ \hat{f}_{\mathrm{d}} = 5.2602,\ \hat{a}_1 = 2000.0\ 1/\mathrm{s}^2,$$
$$\hat{a}_2 = 176.0\ 1/\mathrm{s}. \tag{12}$$

The details of parameter identification were reported in [24]. The same estimated parameters in (12) are used to validate the proposed model through experimental studies in the subsequent subsections. The MATLAB program for the semi-physical model and the experimental data sets are available online for academic studies.[1]

3.3 Comparison with Karnopp model

The updated model (10) for the force-position conversion process has almost the same formulation as the Karnopp model [17,18], except that Stribeck friction is ignored in (10). This subsection, however, shows a major difference between the models. That is, when the valve moves, (10) is an overdamped dynamic system, instead of being the underdamped counterpart in Karnopp model. The overdamped dynamics is in line with experimental observations, while the underdamped dynamics is not.

The physical parameters of Karnopp model are not possible to be identified from experimental data. As a result, the parameters for a nominal pneumatic control valve, reproduced in Table 1, are used in this context. These parameters came from Kayihan and Doyle [18] and had been used in Karnopp model [17,18] and for the

[1] http://www.mech.pku.edu.cn/robot/teacher/wangjiandong/research.htm.

Table 1 Parameters of a nominal pneumatic control valve [18]

Parameter	Description	Value/Unit (SI)
S	Diaphragm area	6.45×10^{-2} m^2
k	Spring constant	5.25×10^4 kg/s^2
m	Mass of stem and plug	1.36 kg
F_{c}	Coulomb friction	1423 kg m/s^2
F_{s}	Static friction	1708 kg m/s^2
F_{v}	Viscous friction coefficient	1.59 kg/s
x_{m}	Valve stroking range	0.1016 m

establishment of He's semi-physical model [9,11]. The corresponding parameters $a_1 := k/m$ and $a_2 := F_{\mathrm{v}}/m$ in (9) are $a_{1n} = 3.8603 \times 10^4$ and $a_{2n} = 1.1691$ for Karnopp model, where the subscript n is used for the ease of comparison.

Assume that the force-position conversion process in (10) has a zero initial state, i.e., $x(t) = 0, \forall\, t < 0$. When the valve moves, without loss of generality in the positive direction with $\dot{x} \geq \delta$, the motion equation in (10) and the counterpart in Karnopp model are the same, i.e.,

$$\ddot{x} = a_1(p_2 - x - f_{\mathrm{d}}) - a_2\dot{x}.$$

Define $p_3(t) := p_2(t) - f_{\mathrm{d}}$. Then, a second-order linear time-invariant system is formulated to be

$$\frac{X(s)}{P_3(s)} = \frac{a_1}{s^2 + a_2 s + a_1}, \tag{13}$$

where $X(s)$ and $P_3(s)$ are the Laplace transforms of $x(t)$ and $p_3(t)$, respectively. The damping coefficient for Karnopp model is

$$\zeta_n = \frac{a_{2n}}{2\sqrt{a_{1n}}} = 0.0030,$$

while its counterpart in (10) by using the parameters identified in (12) is

$$\zeta = \frac{\hat{a}_2}{2\sqrt{\hat{a}_1}} = 1.9677.$$

Since ζ is much larger than ζ_n, the behavior of the proposed model (10) is very different from Karnopp model.

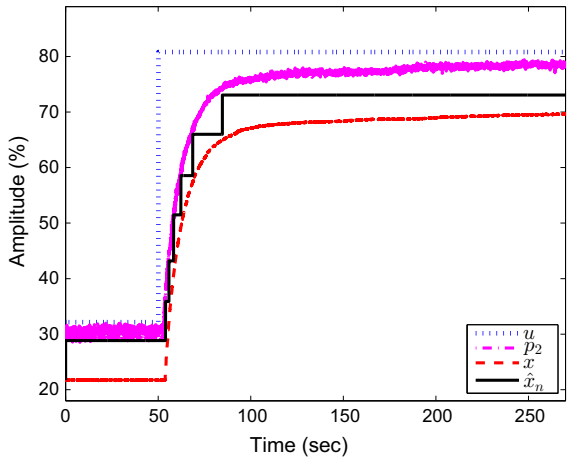

Fig. 7 Signals in a step response experiment for comparison between Karnopp model and experimental observation: the electric control signal u, air pressure p_2 in valve chamber, measured valve position x, and simulated valve position $\hat{x}_n$ from Karnopp model

The proposed model is compared against the Karnopp model in terms of their step responses as follows. The behavior of Karnopp model is inconsistent with our experimental observation shown in Fig. 7. The electric control signal u in Fig. 7 is a step signal with an amplitude 50, which is large enough to overcome the normalized static friction parameter f_s in (9). As expected from (5), the measured air pressure p_2 continuously varies like a step response of a first-order linear dynamic system. The simulated output $\hat{x}_n$ of Karnopp model with a_{2n}, using p_2 as the actual input, is the one in the solid line shown in Fig. 7. Because ζ_n takes a small value, $\hat{x}_n$ shows a jumpy behavior once the valve stem moves. By contrast, the measured valve position x in Fig. 7 monotonically increases and exhibits no jumpy behavior. Thus, x is very different from $\hat{x}_n$, which proves that Karnopp model having the underdamped dynamics is not appropriate for modeling the force-position conversion process in the pneumatic control valve. The movement of x implies that (13) has a damping coefficient much larger than $\zeta_n = 0.0030$. The proposed model having $\zeta = 1.9677$ performs in line with x in the step response experiment, as shown later in Sect. 3.4.1.

3.4 Validation of the proposed model in multiple experiments

This subsection validates the proposed model and compares it with He's semi-physical model and Kano model in multiple experiments. The valve signatures of He's semi-physical model and Kano model are shown in Fig. 8, obtained by using a sinusoidal valve input with sufficiently large amplitudes to overcome the stiction and move the valve stem. Denote He's semi-physical model as

$$x_{\mathrm{H}}(t) = H(u(t); K_1, f_{\mathrm{s1}}, f_{\mathrm{d1}}),$$

where f_{s1} and f_{d1} stand for the static friction and dynamic friction, respectively. The third parameter K_1 takes a default value 1.99 as suggested in [9,11]. Similarly, denote Kano model as

$$x_{\mathrm{K}}(t) = K(u(t); S, J),$$

where S and J are the deadband plus stickband and stickband, respectively. The optimal estimates of f_{s1} and f_{d1} for He's semi-physical model and S and J for Kano model can be obtained by maximizing the fitness value (11), respectively.

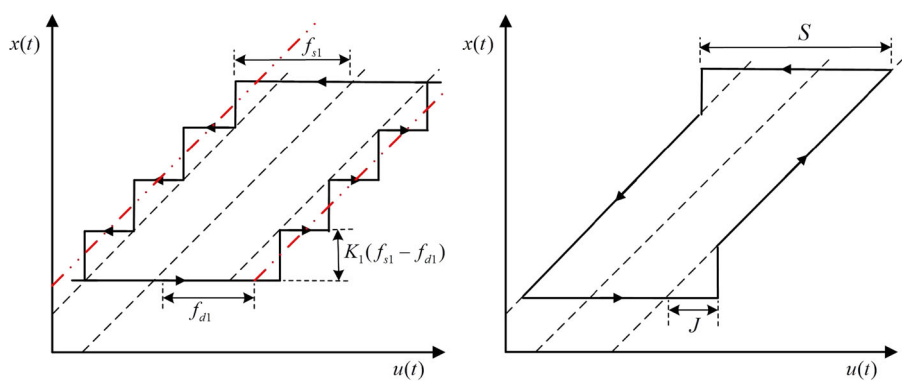

Fig. 8 Valve signatures of He's semi-physical model (*left*, adapted from Fig. 3 in [9]) and Kano model (*right*, adapted from Fig. 2 in [16])

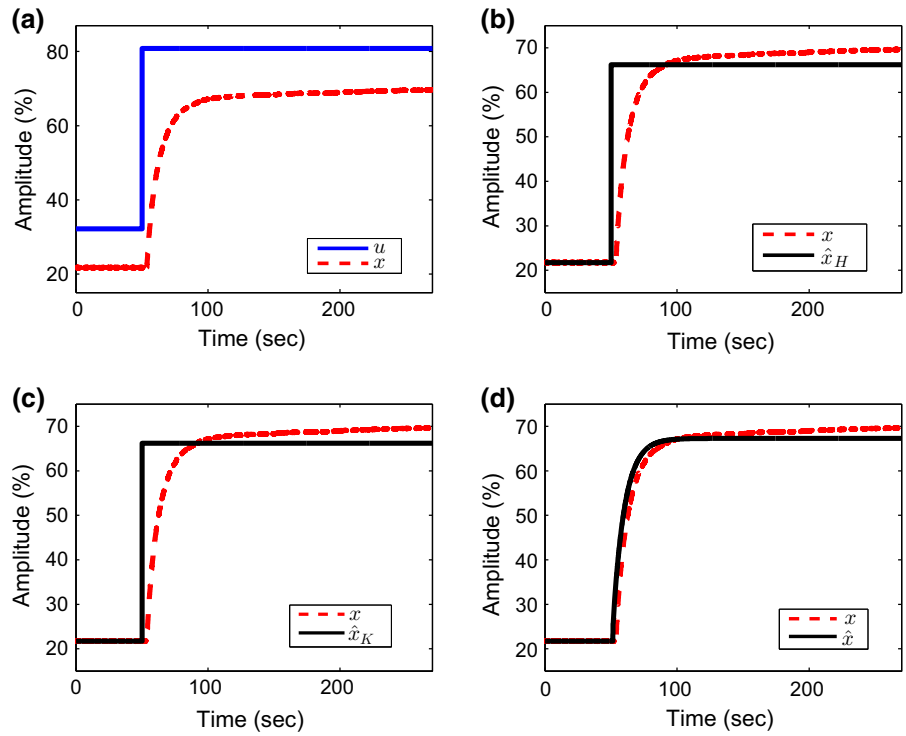

Fig. 9 Signals in a step response experiment: **a** electric control signal u (*solid*), measured valve position x (*dash*); **b** x (*dash*) and simulated valve position $\hat{x}_{\mathrm{H}}$ from He's semi-physical model (*solid*); **c** x (*dash*) and simulated valve position $\hat{x}_{\mathrm{K}}$ from Kano model (*solid*); **d** x (*dash*) and simulated valve position $\hat{x}$ from the proposed model (*solid*)

3.4.1 Step response experiment

The step response experiment is designed for two purposes. First, the step responses of He's semi-physical model, Kano model and the proposed semi-physical model are compared. The step response of the control valve in the experiment is shown in Fig. 9a. The same data are also used for the comparison between Karnopp model and experimental observations in Sect. 3.3. The parameters are estimated as $\hat{f}_{\mathrm{s1}} = 14.5920$ and $\hat{f}_{\mathrm{d1}} = 14.5920$ for He's semi-physical model, and $\hat{S} = 29.1840$ and $\hat{J} = 0$ for Kano model. The fitness value for He's semi-physical model and Kano model is the same, equal to 58.1071 %, while its counterpart for the proposed semi-physical model using the parameters in (12) is 87.7564 %. Figure 9b–d present the simulated valve positions $\hat{x}_{\mathrm{H}}$ from He's semi-physical model, $\hat{x}_{\mathrm{K}}$ from Kano model and $\hat{x}$ from the proposed model, respectively. Clearly, the proposed model can match well the step response of the actual control valve, while He's semi-physical model and Kano model exhibit a jumpy behavior that is very different from the experimental observations.

Second, multiple step responses are implemented. The steady-state values of p_2 in the step responses are plotted against u in Fig. 10. It proves the existence of the backlash nonlinearity in (1) between u and p_1 in the electric-pneumatic conversion process. Note that p_1 and p_2 are equal in the steady state.

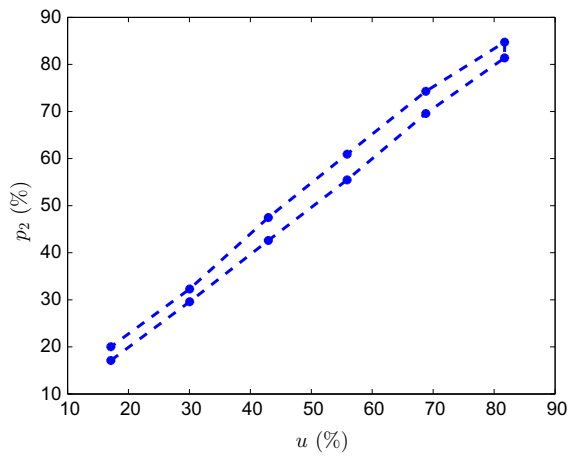

Fig. 10 The steady-state values of p_2 versus u in the step response experiments

3.4.2 Short-time impulse experiment

The short-time impulse experiment is to show the behavior of the three models in response to a short-

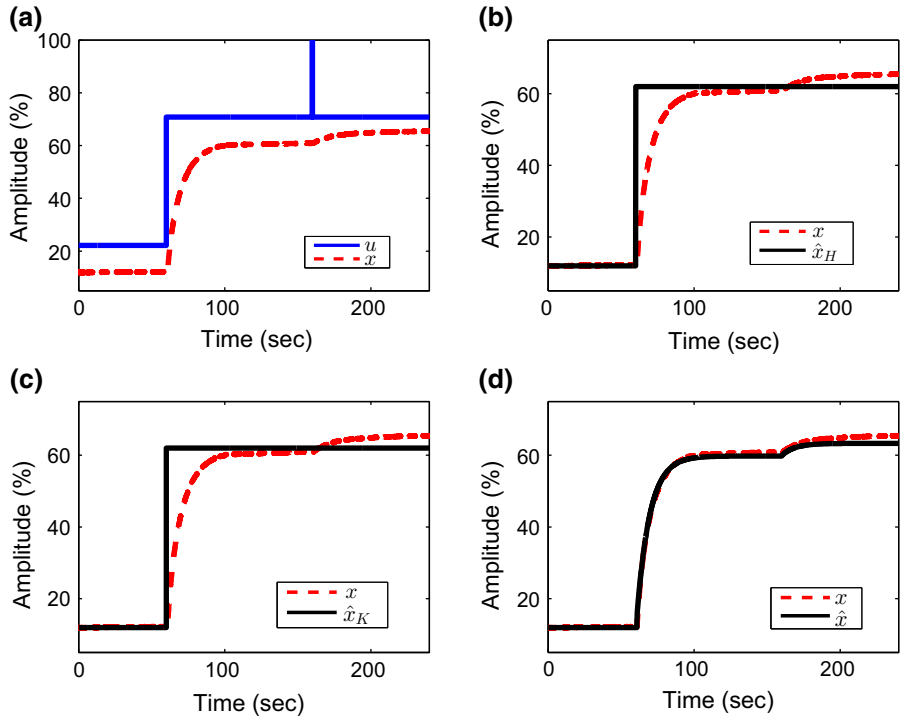

Fig. 11 Signals in a short-time impulse experiment: **a** electric control signal u (*solid*), measured valve position x (*dash*); **b** x (*dash*) and simulated valve position $\hat{x}_{\mathrm{H}}$ from He's semi-physical model (*solid*); **c** x (*dash*) and simulated valve position $\hat{x}_{\mathrm{K}}$ from Kano model (*solid*); **d** x (*dash*) and simulated valve position $\hat{x}$ from the proposed model (*solid*)

time large variation of the input, as well as the existence of the backlash nonlinearity in (1). The input u is designed as a short-time impulse signal with amplitude 30 and duration of two sampling periods. The measurements u and x are presented in Fig. 11. The stiction parameters of He's semi-physical and Kano models are $\hat{f}_{\mathrm{s1}} = 39.5280$, $\hat{f}_{\mathrm{d1}} = 24.0788$, $\hat{S} = 48.3120$, and $\hat{J} = 30.7440$. The reason to repeat the identification procedure for He's semi-physical model and Kano model, instead of using the identified parameters in Sect. 3.4.1, is to achieve their best fitness performances under the current circumstance. The simulated valve positions $\hat{x}_{\mathrm{H}}$, $\hat{x}_{\mathrm{K}}$ and $\hat{x}$ are shown in Fig. 11. He's semi-physical model and Kano model share the same fitness 64.8389 %, while the fitness for the proposed semi-physical model is 95.1610 %. Figure 11 demonstrates that only $\hat{x}$ follows the dynamic variation of x after the short-time impulse of u, which also supports the backlash nonlinearity in (1). By contrast, $\hat{x}_{\mathrm{H}}$ and $\hat{x}_{\mathrm{K}}$ have no movements after the short-time impulse.

3.4.3 Cosine input experiment

This experiment presents the frequency response of the proposed semi-physical model. The input is a cosine signal with a gradually decreasing frequency, as shown in Fig. 12. The estimated parameters of He's semi-physical model and Kano model are $\hat{f}_{\mathrm{s1}} = 24.3200$, $\hat{f}_{\mathrm{d1}} = 22.7924$, $\hat{S} = 45.6000$, and $\hat{J} = 1.8240$. The simulated valve positions $\hat{x}_{\mathrm{H}}$, $\hat{x}_{\mathrm{K}}$ and $\hat{x}$ are shown in Fig. 12. He's semi-physical model and Kano model yield the fitness values 49.9765 and 52.6920 %, respectively, while the proposed semi-physical model gives a larger fitness 76.2387 %. More importantly, $\hat{x}_{\mathrm{H}}$, $\hat{x}_{\mathrm{K}}$ are oscillating with the constant maximum and minimum values, which are very different from the amplitude variations of x. By contrast, $\hat{x}$ can reproduce more accurately the variation of x. In particular, the asymmetric behavior for the increment and decrement parts of x supports the input-direction-dependent dynamics in (5).

3.4.4 Closed-loop experiment

This experiment illustrates the behavior of the control valve and the three models in a closed-control loop operation. The valve position x is compared with a reference signal r. Their difference is the input of a proportional-integral controller $C(s) = 0.2083\left(1 + \frac{1}{15s}\right)$ implemented in Matlab® platform

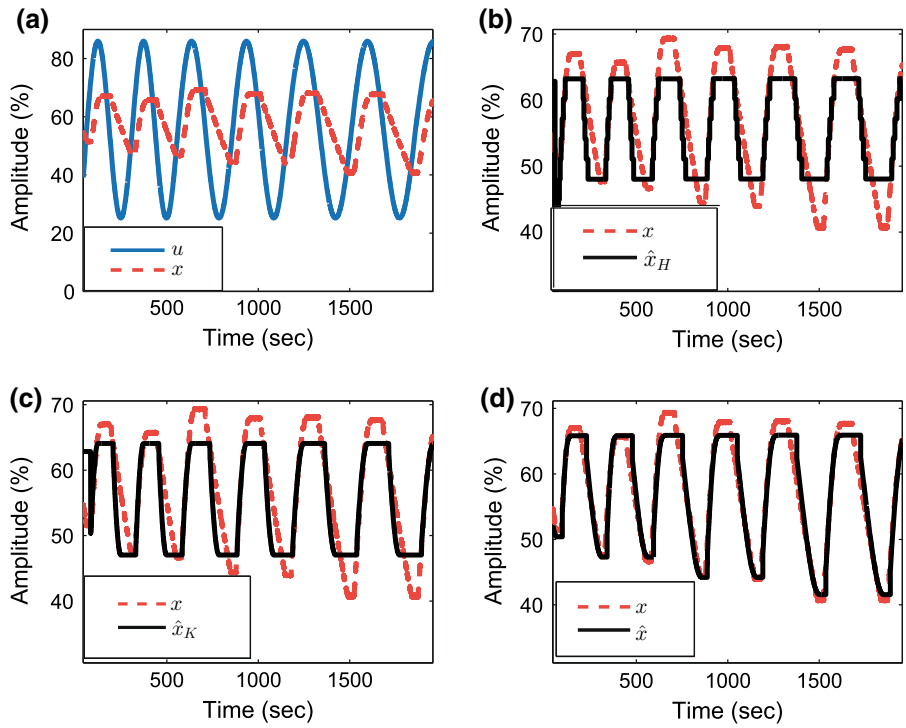

Fig. 12 Signals in a cosine input impulse experiment: **a** electric control signal u (*solid*), measured valve position x (*dash*); **b** x (*dash*) and simulated valve position $\hat{x}_{\mathrm{H}}$ from He's semi-physical model (*solid*); **c** x (*dash*) and simulated valve position $\hat{x}_{\mathrm{K}}$ from Kano model (*solid*); **d** x (*dash*) and simulated valve position $\hat{x}$ from the proposed model (*solid*)

with sampling period $T_{\mathrm{s}} = 0.02\,\mathrm{s}$. The controller output is sent to the valve positioner as u. The setpoint r of the control loop, controller output u and valve position x in the experiment are shown in Fig. 13. The parameters are estimated to be $\hat{f}_{\mathrm{s1}} = 25.9259$, $\hat{f}_{\mathrm{d1}} = 21.8118$ for He's semi-physical model with the fitness value 56.9552 %, and $\hat{S} = 25.0$, and $\hat{J} = 2.0$ for Kano model with the fitness value −22.6468 %. The fitness for the proposed semi-physical model using the parameters in (12) is 79.6304 %. The simulated valve positions $\hat{x}_{\mathrm{H}}$, $\hat{x}_{\mathrm{K}}$ and $\hat{x}$ are presented in Fig. 13. In the experiment, the valve position x continuously changes. However, $\hat{x}_{\mathrm{H}}$ and $\hat{x}_{\mathrm{K}}$ fail in following x by only showing one abrupt jump, while $\hat{x}$ fits x very well. Note that the estimated He's semi-physical and Kano models are different in the steady-state values of $\hat{x}_{\mathrm{H}}$ and $\hat{x}_{\mathrm{K}}$.

The above experiments strongly demonstrate the existence of the backlash nonlinearity (1) in the electric-pneumatic conversion process, the input-direction-dependent linear dynamics (5) in the pneumatic-force conversion process, and the overdamped nonlinear dynamics (10) in the force-position conversion process. The large discrepancies between the measured valve positions and the estimated ones from He's semi-physical model and Kano model are observed, which mainly is due to the fact that they only model the force-position conversion process, and thus cannot fully describe the behavior of a pneumatic control valve involving three signal conversion processes from u to x.

4 Conclusions

In this paper, the semi-physical model in Fig. 5 was proposed for pneumatic control valves, based on physical principles of three signal conversion processes, namely, the electric-pneumatic conversion process in the valve positioner, the pneumatic-force conversion process in the valve actuator, and the force-position conversion process in the valve body. Compared with the related models in the literature, the proposed semi-physical model has two new components, namely, the backlash nonlinearity (1) in the electric-pneumatic conversion process, and the input-direction-dependent dynamics (5) in the pneumatic-force conversion process; in addition, the nonlinear model (10) in the force-position conversion process has a much larger damping coefficient, and becomes an overdamped dynamic system when the valve moves. These differences are the funda-

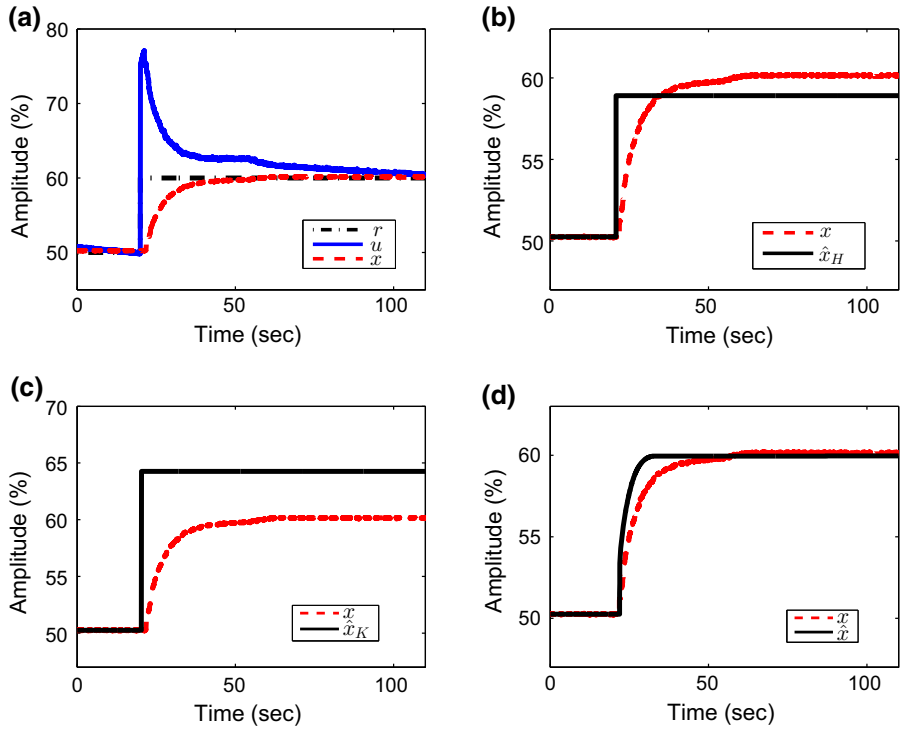

Fig. 13 Signals in a closed-loop experiment: **a** setpoint r (*dot-dash*), electric control signal u (*solid*), measured valve position x (*dash*); **b** x (*dash*) and simulated valve position $\hat{x}_H$ from He's semi-physical model (*solid*); **c** x (*dash*) and simulated valve position $\hat{x}_K$ from Kano model (*solid*); **d** x (*dash*) and simulated valve position $\hat{x}$ from the proposed model (*solid*)

mental reasons why the proposed semi-physical model behaves consistently with experimental results of the actual pneumatic control valve, while the representative models in the literature have large discrepancies.

Based on the experimental studies, we have also noticed some limitations of the proposed semi-physical model to be improved in future works. For instance, there are still some discrepancies between the actual valve position and the simulated one from the proposed model, which needs to be improved. One possibility for improvement is to relieve the assumption that the chamber volume is constant, and build up a more flexible model considering the coupling between the variations of the chamber volume and valve position. Moreover, owing to the limited experimental devices, only one pneumatic control valve was investigated to validate the proposed model; thus, another future work is to perform experimental studies of the proposed model based on more pneumatic control valves.

References

1. Armstrong, B.H., Dupont, P., De Wit, C.C.: A survey of models, analysis tools and compensation methods for the control of machines with friction. Automatica **30**(7), 1083–1138 (1994)
2. Bialkowski, W.L.: Dreams versus reality: a view from both sides of the gap. Pulp Pap. Can. **94**, 19–27 (1993)
3. Chen, S.L., Tan, K.K., Huang, S.: Two-layer binary tree data-driven model for valve stiction. Ind. Eng. Chem. Res. **47**(8), 2842–2848 (2008)
4. Choudhury, M.A.A.S., Thornhill, N.F., Shah, S.L.: Modelling valve stiction. Control Eng. Pract. **13**(5), 641–658 (2005)
5. De Wit, C.C., Olsson, H., Astrom, K.J., Lischinsky, P.: A new model for control of systems with friction. IEEE Trans. Autom. Control **40**(3), 419–425 (1995)
6. Desborough, L., Nordh, P., Miller, P.: Control system reliability: process out of control. Ind. Comput. **8**, 52–55 (2001)
7. Garcia, C.: Comparison of friction models applied to a control valve. Control Eng. Pract. **16**(10), 1231–1243 (2008)
8. Harrold, D.: Making valve controllers/positioners smarter is smart business. Control Eng. **50**(1), 24–30 (2003)
9. He, Q.P., Wang, J.: Valve stiction quantification method based on a semiphysical valve stiction model. Ind. Eng. Chem. Res. **53**(30), 12010–12022 (2014)
10. He, Q.P., Wang, J., Pottmann, M., Qin, S.J.: A curve fitting method for detecting valve stiction in oscillating control loops. Ind. Eng. Chem. Res. **46**(13), 4549–4560 (2007)
11. He, Q.P., Wang, J., Qin, S.J.: An alternative stiction-modelling approach and comparison of different stiction models, chap 3. Springer, Berlin (2010)
12. ISA: Control valve diagnostic data acquistion and reporting. Standard ANSI/ISA-752601-2006 (2006)

13. Isermann, R.: Fault-Diagnosis Applications: Model-Based Condition Monitoring: Actuators, Drives, Machinery, Plants, Sensors, and Fault-Tolerant Systems. Springer, Berlin (2011)
14. Jeffery, H.: Loop Checking: A Technician's Guide. ISA, New York (2005)
15. Jelali, M., Huang, B.: Detection and Diagnosis of Stiction in Control Loops: State of the Art and Advanced Methods. Springer, Berlin (2010)
16. Kano, M., Maruta, H., Kugemoto, H., Shimizu, K.: Practical model and detection algorithm for valve stiction. In: IFAC Symposium on Dynamics and Control of Process Systems pp. 5–7 (2004)
17. Karnopp, D.: Computer simulation of stick-slip friction in mechanical dynamic systems. J. Dyn. Syst. Meas. Control **107**(1), 100–103 (1985)
18. Kayihan, A., Doyle, F.: Friction compensation for a process control valve. Control Eng. Pract. **8**, 799–812 (2000)
19. Liptak, B.G. (ed.): Instrument Engineers' Handbook. CRC Press, Boca Raton (2003)
20. Olsson, H.: Control systems with friction. Ph.D. thesis, Lund University (1996)
21. Olsson, H., Astrom, K.J., De Wit, C.C., Gafvert, M., Lischinsky, P.: Friction models and friction compensation. Eur. J. Control **4**(3), 176–195 (1998)
22. Stenman, A., Gustafsson, F., Forsman, K.: A segmentation-based method for detection of stiction in control valves. Int. J. Adapt. Control Signal Process. **17**(7–9), 625–634 (2003)
23. Sutera, S.P., Skalak, R.: The history of poiseuille's law. Ann. Rev. Fluid Mech. **25**(1), 1–20 (1993)
24. Tang, L., Fang, L., Wang, J., Shang, Q.: Modeling and identification for pneumatic control valves with stiction. In: 17th IFAC Symposium on System Identification, pp. 1244–1249 (2015)
25. Xie, L., Cong, Y., Horch, A.: An improved valve stiction simulation model based on ISA standard tests. Control Eng. Pract. **21**(10), 1359–1368 (2013)